NUMERICAL SIMULATIONS OF FLOWS OF A SMD FLUID VIA THE GALERKIN LEAST-SQUARES METHOD

Ana Paula Schwarz, apschwarz@mecanica.ufrgs.br
Flávia Zinani, fla@mecanica.ufrgs.br
Sérgio Frey[1], frey@mecanica.ufrgs.br
Laboratory of Computational and Applied Fluid Mechanics (LAMAC) - Mechanical Engineering Department- Federal University of Rio Grande do Sul - Rua Sarmento Leite, 425 - 90050-170 – Porto Alegre, RS, Brazil

Abstract. *The main objective of this paper consists of numerical simulations of viscoplastic fluid flows using the finite element method. The mechanical modeling employed is based on the mass and momentum conservative equations coupled with the constitutive model recently proposed by Souza Mendes Dutra - herein only named by SMD. The mechanical modeling was approximated via the Galerkin Least-Squares method (GLS) which is built to overcome the numerical shortcoming of the classical Galerkin method for mixed formulations without damaging its consistency. First, in order to check the computational code, a Newtonain leaky cavity flow has been approximatied for the Stokes problem. Next, two viscoplastic fluid flows has been considered: a SMD fluid flow through an sudden expansion followed by a contraction geometry - for 0.4<n<0.9 and 1<J<10⁶- and around a circular cylinder - for $0.1 < \overline{u}^* < 2.5$. The numerical results generated gave some physical information on the viscoplastic phenomena studied and are in accordance with the literature.*

Keywords: Viscoplasticity, SMD fluid; expansion and contraction flow, flow around a cylinder, Galerkin least-squares method.

1. INTRODUCTION

A viscous fluid flow is a thermodynamical process of irreversible deformation. In order to characterize viscous properties of the flowing fluid on has to consider to dynamical and kinematical aspects of the deformation. The local characterization of the dynamical and kinematical states of the flowing fluid is respectively given by the stress and rate of strain tensors.

The problem immensely simplifies if we limit ourselves to flows which are a non-zero component of velocity in only a single direction - that is, the so-called pure shear flows. For these flows, the measure of the local dynamic and kinematical states of deformation is the shear stress and the shear rate, respectively. During the shear flow of a Newtonian fluid, these two quantities are related by the linear Newtonian law of viscosity (Slattery, 1999).

It has to be mentioned that the fulfillment of the Newton law is not the only requirement for a fluid be classified as a Newtonian one. The fluid may not exhibit memory effects resulting from elasticity or/and thixotropy, the first and second normal stress differences of the fluid is equal to zero, the ratio of the extensional to shear viscosity is constant. If any of these requirements is not fulfill the fluid is said to be non-Newtonian.

In industrially important situations non-Newtonian fluids may exhibit very complicated rheological behavior. From the pragmatic point of view, however, the decisive property of the fluid is often its variable viscosity which changes with shear rate, which, for some fluids, may change in a very broad range indeed.

The simplest approach the non-Newtonian viscosity is given by the generalization of linear Newton law in the following way (Astarita and Marrucci, 1974)

$$\eta(\dot\gamma) = \frac{\tau}{\dot\gamma} \tag{1}$$

where the η dependent on the magnitude of the rate of strain tensor, $\dot\gamma$, and τ is the magnitude of the shear stress tensor.

In order to describe the dependence of viscosity η on shear rate $\dot\gamma$, the so-called viscosity functions $\eta(\dot\gamma)$ are used. To capture shear-thinning and shear-thickening features, the Ostwald-Waele power-law fluid and the Carreau fluid are the most employed. If the material exhibits some shear limit in order to flow, the Bingham plastic, the Herschel-Buckley and Casson models may be considered (Bird et al., 1987).

This article performs finite element simulations of steady-state isochoric flows of a viscoplastic fluid recently proposed by Souza Mendes and Dutra (2004) – henceforth named SMD fluid. In order to carry out the numerical tests, a Galerkin least-squares formulation has been introduced. Three fluid flows have been considered. First of all, in order to check the computational code, the leaky cavity flow of a linear Newtonian fluid has been approximated, for Reynolds

---

[1] Correspondence author.

number equals zero. Following, a SMD fluid flow was studied flowing in two distinct situations: through a sudden expansion and contraction axisymmetric geometry - for power law exponent varied from 0.4 to 0.9 and the jump number from 1 to 10^6 - and around a circular cylinder - for the dimensionless average velocity of the fluid at the channel inlet raged from 0.1 to 2.5.

2. MECHANICAL MODDELING

The mechanical of non-Newtonian fluids is the study of the fluid material behavior when at flow. The analysis of the involved phenomena is based on the simultaneous solution of a certain number of governing equations of representative physical laws. These equations may be grouped in two distinct categories. The first one includes the equations representing certain physical laws that are supposed valid for all mechanical bodies – the so-called balance equations. These equations mathematically express the four major conservative principle in Mechanics, e.g., the conservative principle of mass, momentum, angular momentum and energy.

2.1 Balance equation

2.1.1 Principle of mass conservation

The principle mass conservation is express by: "the net afflux of mass that enters in the fluid system Ω is equal to the mass increase in the interior of Ω". The Eulerian form of this principle may be written as (Slattery, 1999),

$$\partial_{,t}\rho + \mathrm{div}(\rho\mathbf{v}) = 0 \tag{2}$$

where ρ is the fluid density and $\mathbf{v}$ the fluid velocity.

For constant density fluids, Eq. (2) reduces to

$$\mathrm{div}\,\mathbf{v} = 0 \tag{3}$$

2.1.2 Principle of momentum conservation

For a given fluid system Ω, the principle of momentum conservation may be stated as: "the net afflux of momentum that enters in the system Ω added to the resultants of gravitational and contact forces acting on it, is equal to the rate of momentum increase in the interior of Ω". Its Eulerian form may be express by (Slattery, 1999)

$$\rho\left(\partial_t\mathbf{v} + [\nabla\mathbf{v}]\mathbf{v}\right) = -\nabla p + \mathrm{div}\,\boldsymbol{\tau} + \rho\mathbf{g} \tag{4}$$

where p is the pressure field, $\boldsymbol{\tau}$ the deviatory tensor and $\mathbf{g}$ the gravity acceleration.

2.1.3 Constitutive equations

Constitutive equations belong to a class of equations representing some physical laws which govern the mechanical behavior of a particular material. The form of these equations depends on the material class considered, with their parameter values depending on the specific material studied. For the general case, it must be imposed a thermodynamic equation of state for the pressure field, a constitutive equation for the stress tensor, a heat transfer equation for the heat flux and a energetic equation of state for the internal energy of the material (Astarita, and Marrucci., 1974). For the isothermal flows of constant density fluids, only the first equations must be considered.

For a Newtonian incompressible fluid, the constitutive equation for the stress tensor is given by

$$\mathbf{T} = -p\mathbf{1} + 2\mu\mathbf{D} \tag{5}$$

where p is defined as previously, $\mathbf{1}$ the unit tensor, μ the constant fluid viscosity and $\mathbf{D}$ the rate of strain tensor.

In order to add some shear-thinning feature to Eq.(5), a generalized Newtonian viscosity function $\eta(\dot{\gamma})$ - as defined by Eq. (1) - may be introduced in Eq. (5)

$$\mathbf{T} = -p\mathbf{1} + 2\eta(\dot{\gamma})\mathbf{D} \tag{6}$$

As examples of well-known shear-thinning models it must be cited the power-law and Carreau equations (Bird et al., 1987).

Now, in order to accommodate the viscoplastic behavior into the shear-thinning model defined by Eq. (5), a yield stress limit τ_0 may be considered, below which the fluid will not flow. As already depicted in the introductory section of this article, the Bingham plastic and Herschel-Bulkley, and Casson equations are classical examples of viscoplastic models (Bird et al., 1987).

In this work, the SMD viscoplastic model was the one proposed by Souza Mendes and Dutra (2004) has been adopted. This model may be mathematically express by the following equation,

$$\tau = \left(1 - \exp\left(-\eta_o \dot{\gamma} / \tau_o\right)\right)\left(\tau_o + K\dot{\gamma}^n\right) \tag{7}$$

where $\dot{\gamma}$ and τ and τ_0 are defined as previously, η_0 is the zero-shear-rate viscosity, K consistency index and n the power-law exponent. From Equation (7), the SMD viscosity function is given by

$$\eta(\dot{\gamma}) = \left(1 - \exp\left(-\eta_o \dot{\gamma} / \tau_o\right)\right)\left(\frac{\tau_o}{\dot{\gamma}} + K\dot{\gamma}^{n-1}\right) \tag{8}$$

where $\dot{\gamma}$, $\eta(\dot{\gamma})$, τ_0, η_0, K and n are defined as previously.

A dimensionless rheological property for viscoplastic fluids introduced by Souza Mendes et al. (2007) is the so-called jump number, J, which provides the relative measure of the shear rate jump when the shear stress is approximately equals to the limit stress, τ_0. Mathematically, it may be defined by

$$J \equiv \frac{\dot{\gamma}_1 - \dot{\gamma}_o}{\dot{\gamma}_o} \tag{9}$$

where $\dot{\gamma}_o$ and $\dot{\gamma}_1$ are respectively the shear rate values at the beginning of the shear rate jump and the power-law region, i. e., $\dot{\gamma}_o \equiv \dfrac{\tau_o}{\eta_o}$ and $\dot{\gamma}_1 \equiv \left(\dfrac{\tau_o}{K}\right)^{1/n}$. Hence, from Eq. (9), one obtains

$$J = \frac{\eta_o \left(\tau_o\right)^{(1-n)/n}}{\left(K\right)^{1/n}} - 1 \tag{10}$$

where η_0, τ_0, K and n are defined as previously.
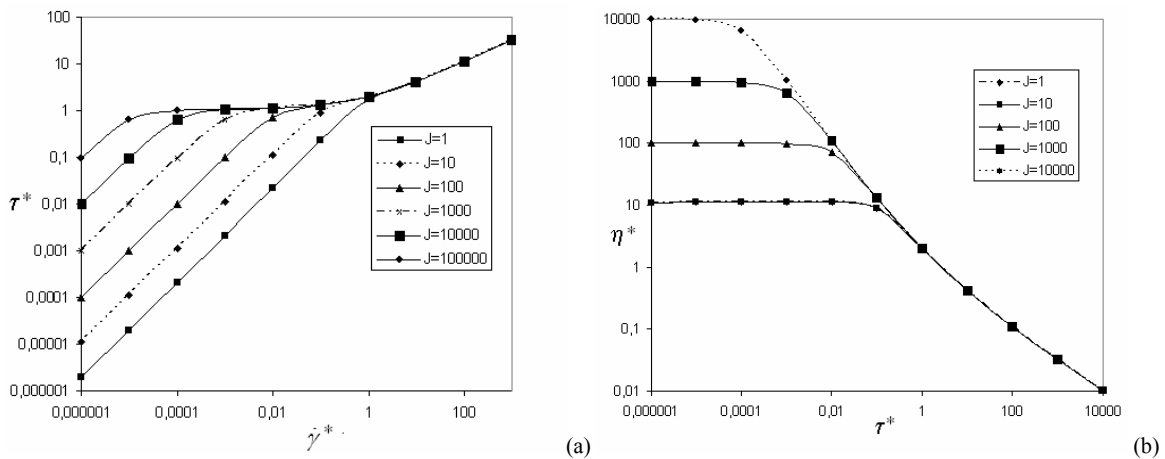
Figure 1. SMD model for n=0.5: (a) Flow charter; (b) SMD viscosity function.

The Figure 1 shows the flow charter (Fig. 1(a)) and viscosity function of SMD model (Fig. 1(b)). It may be seen that the relative measure of the shear rate jump augments with the jump number increase, i.e., the shear rate increases while the shear stress approximately remains equal to τ_0 until the beginning of the power-law region.

3. FINITE ELEMENTS APROXIMATION

Suppose a flow domain $\Omega \subset \Re^2$ with regular boundary Γ. Based on the continuity (Eq. (2)) and motion (Eq. (4)) equations coupled to the GNL constitutive equation (Eq. (6)), the steady-state flows of incompressible fluids may be modeled by the following boundary-valued problem,

$$\rho\left(\left[\nabla \mathbf{v}\right]\mathbf{v}\right) = -\nabla p + 2\eta\left(\dot{\gamma}\right)\mathrm{div}\mathbf{D}(\mathbf{u}) + \rho\mathbf{g} \quad \text{in } \Omega$$
$$0 = \mathrm{div}\mathbf{u} \quad \text{in } \Omega$$
$$\mathbf{u} = \mathbf{u}_g \quad \text{on } \Gamma_g \tag{11}$$
$$\mathbf{Tn} = \mathbf{t_n} \quad \text{on } \Gamma_h$$

where $\rho, p, \eta(\dot{\gamma})$, $\mathbf{D}$, $\mathbf{g}$ are defined as previously, $\mathbf{u}$ and $\mathbf{v}$ are respectively the admissible and virtual velocities, $\mathbf{n}$ the outward unit vector, $\mathbf{t_n}$ the stress vector, Γ_g and Γ_h the regions of boundary Γ on which Dirichlet and Neumann conditions was imposed and the stress tensor $\mathbf{T}$ given by Eq. (6) and (7).

3.1 Variational formulation

Thus, taking the dot product between the continuity and motion equations (defined by Eq. (11)) and a virtual velocity and pressure ($\mathbf{v}$,q), respectively, the variational formulation for Eq. (11) may be written as: given the fluid density ρ, the body and contact forces $\mathbf{g}$ and $\mathbf{t_n}$, respectively, and Dirichlet boundary condition $\mathbf{u}_g$, find the pair $(\mathbf{u},q) \in H^1(\Omega) \times L_2(\Omega)$ such that

$$\int_\Omega \rho\left(\left[\mathrm{grad}\mathbf{v}\right]\mathbf{v}\right)\bullet\mathbf{v}d\Omega + \int_\Omega 2\eta\left(\dot{\gamma}\right)\mathbf{D}(\mathbf{u})\bullet\mathbf{D}(\mathbf{v})d\Omega - \int_\Omega p\,\mathrm{div}\mathbf{v}d\Omega - \int_\Omega \mathrm{div}\mathbf{u}\,qd\Omega = \int_\Omega \rho\mathbf{g}\bullet\mathbf{v}d\Omega, \ \forall\left(\mathbf{v},q\right) \in H_0^1\left(\Omega\right) \times L_2\left(\Omega\right) \tag{12}$$

where Ω, ρ, p, q, $\mathbf{u}, \mathbf{v}, \eta(\dot{\gamma})$, $\mathbf{D}$, $\mathbf{g}$ are defined as previously and the functional spaces $L_2(\Omega)$ and $H^1(\Omega)$ are given by:

$$L_2\left(\Omega\right) = \{\ q\ |\ \int_\Omega q^2 d\Omega\ <\ \infty\}$$
$$H^1\left(\Omega\right) = \left\{v\ \in\ L_2\left(\Omega\right)|\ \partial v/\partial x_i \in L_2\left(\Omega\right)\}, \ i = 1, N\right\} \tag{13}$$

3.2 Galerkin least-squares approximation

The finite element approximation of Eq. (12) may be built by employing the usual fluid dynamics subspaces for velocity ($\mathbf{V}_h$) and pressure (P_h),

$$\mathbf{V}_h = \{\mathbf{v} \in H_0^1(\Omega)^N \left| \mathbf{v}_{|K} \in R_k(K)^N, K \in \Omega_h\right.\}$$
$$P_h = \{p \in C^0(\Omega) \cap L_0^2(\Omega) \left| p_{|K} \in R_l(K), K \in \Omega_h\right.\} \tag{14}$$
$$\mathbf{V}_h^g = \{\mathbf{v} \in H^1(\Omega)^N \left| \mathbf{v}_{|K} \in R_k(K)^N, K \in \Omega_h, \mathbf{v} = \mathbf{u}_g \text{ on } \Gamma_g\right.\}$$

with R_k and R_l denoting respectively polynomial spaces of degree k and l (Ciarlet, 1978) and the Sobolev space $H_0^1(\Omega)$ is given by

$$H_0^1(\Omega) = \left\{v\ \in\ L^2(\Omega)|\ \partial v/\partial x_i \in L^2(\Omega)|\ v = 0 \text{ on } \Gamma_g, \ i = 1, N\right\} \tag{15}$$

Based on the above definitions of velocity and pressure subspaces, Eq. (14), a Galerkin least squares (GLS) formulation for steady-state viscoplastic flows may be stated as: given the functions ρ, $\mathbf{g}$, $\mathbf{t_n}$, $\mathbf{u}_g$, find the pair $(\mathbf{u},q) \in \mathbf{V}_h \times P_h$ such that,

$$\rho([\text{grad } \mathbf{u}]\mathbf{u}, \mathbf{v}) + (2\eta(\dot{\gamma})\mathbf{D}(\mathbf{u}), \mathbf{D}(\mathbf{v})) - (p, \text{div } \mathbf{v}) - (q, \text{div } \mathbf{u}) +$$

$$+ \sum_{K \in C_h} \left(\rho[\text{grad } \mathbf{u}]\mathbf{u} + \text{grad } p - 2\,\text{div}\left(\eta(\dot{\gamma})\mathbf{D}(\mathbf{u})\right), \tau(\text{Re}_K)(\rho[\text{grad } \mathbf{v}]\mathbf{u} - 2\,\text{div}\left(\eta(\dot{\gamma})\mathbf{D}(\mathbf{v})\right) - \text{grad } q) \right)_K = \qquad (16)$$

$$= (\rho\mathbf{g}, \mathbf{v}) + (\mathbf{t_n} \cdot \mathbf{v})_{\Gamma_h} + \sum_{K \in C_h} \left(\rho\mathbf{g}, \tau(\text{Re}_K)(\rho[\text{grad } \mathbf{v}]\mathbf{u} - 2\,\text{div}\left(\eta(\dot{\gamma})\mathbf{D}(\mathbf{v})\right) - \text{grad } q) \right)_K$$

where Ω, ρ, p, q, $\mathbf{u}$, $\mathbf{v}$, $\eta(\dot{\gamma})$, $\mathbf{D}$, $\mathbf{g}$ are defined as previously, with the grid Reynolds number Re_K and the stabilized parameter $\tau(\text{Re}_K)$ defined as in Franca and Frey (1992),

$$\tau(\text{Re}_K) = \frac{h_K}{2|\mathbf{u}|_p}\xi(\text{Re}_K) \quad \text{with} \quad \xi(\text{Re}_K) = \begin{cases} \text{Re}_K, 0 \le \text{Re}_K < 1 \\ 1, \text{Re}_K \ge 1 \end{cases} \quad \text{and} \quad \text{Re}_K = \frac{\rho h_K |\mathbf{u}|_p}{2\eta(\dot{\gamma})} \qquad (17)$$

4. NUMERICS RESULTS

In this section, it will be presented the GLS approximations for leaky cavity flow of Newtonian fluid and a sudden expansion and contraction flow of a SMD fluid. All results were obtained employing a finite element code under development at Laboratory of Computational and Applied Fluid Mechanics (LAMAC) of Rio Grande do Sul.

4.1 Newtonian leaky cavity flow

In order to validate the finite element code, it were performed GLS approximations, defined by Eq. (16)-(17), for the leaky cavity flow of a Newtonian fluid. Choosing a rectangular Cartesian coordinate system with its origin on the left corner of a biunity cavity, the numerical simulations were carried out by a Reynolds number equals to zero (see Fig. 2). The velocity boundary conditions imposed were no-slip and impermeability on the cavity walls, but the superior one when a uniform parallel unit velocity has been prescribed. The computational domain Ω_h was partitioned in 10^4 uniform bilinear finite elements (Q1/Q1) generating 6296 nodal points.
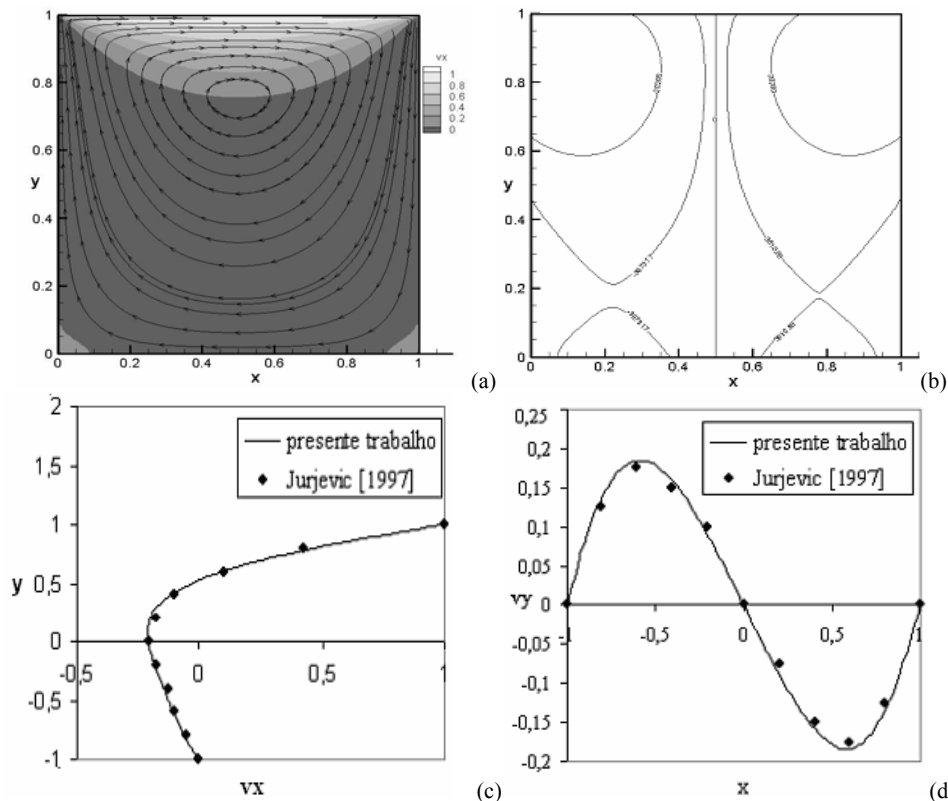
Figure 2. Leaky cavity flow for Re=0: (a) Streamlines; (b) pressure contours; (c) v_x-profile; (d) v_y-profile.

In the Figure 2 was shown the flow streamlines, pressure contours and horizontal and vertical velocity profiles for Re=0. As it may be noticed, the pressure fields were sufficient stable (Fig. 2(b)) and the main vortex was positioned at x=0.5-symmetry line. Figures 2(c) and 2(d) provide the horizontal (v_x) and vertical (v_y) velocity profile comparisons. Both figures present an excellent agreement with the results introduced by Jurjevic (1997) for the Stokes flow problem.

4.2 SMD fluid flow through a duct subjected to a sudden expansion followed by a sudden contraction

In this section, it was performed GLS approximations, defined by Eq. (16)-(17), for the fluid flows suggested in Souza Mendes et al., (2007). The problem statement was illustrated in Fig. 3(a) for a cylindrical polar coordinate with origin at the entrance of the duct (In order to save computational memory, only one half of the domain was considered.). The velocity boundary conditions were no-slip and impermeability on the duct walls, a uniform parallel unit velocity on the duct entrance, free traction on the exit and symmetry boundary conditions at centerline ($\partial_r u_z = u_r = 0$). In the finite element partitioning Ω_h, four distinct meshes were studied: Mesh #1 with 2,164 bilinear finite elements (Q1/Q1); Mesh #2 with 5,969 Q1/Q1 elements; Mesh #3 with 9,568 Q1/Q1 elements and Mesh #4 with 11,664 Q1/Q1 elements.
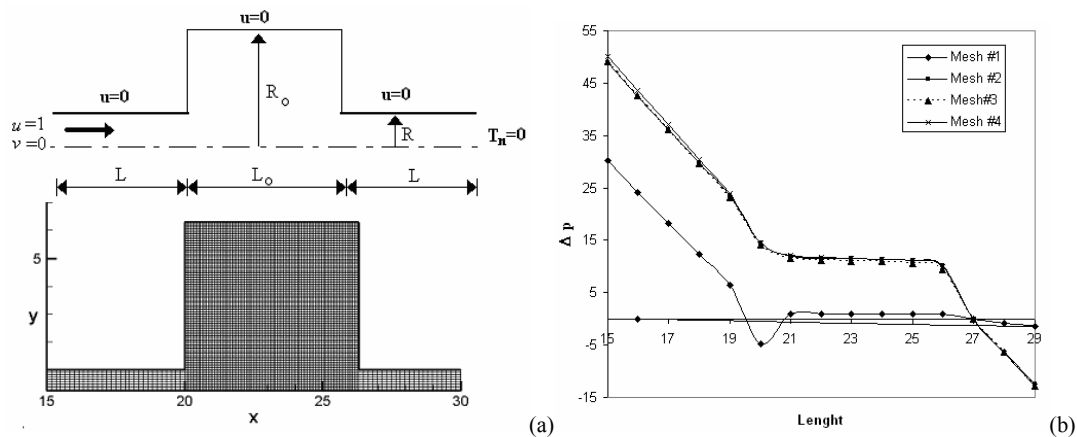
Figure 3. Sudden expansion and contraction flow: (a) problem statement and employed mesh (Mesh#3); (b) mesh independence test.

The duct aspect ratio was defined as relationship between radii R_0 and R (see problem statement (Fig. 3(a)) and was taken as 6.3. In the numerical simulations performed, the jump number (Eq. (10)) was ranged from 1 to 10^5 and the power-law exponent was taken from 0.4 to 0.9.
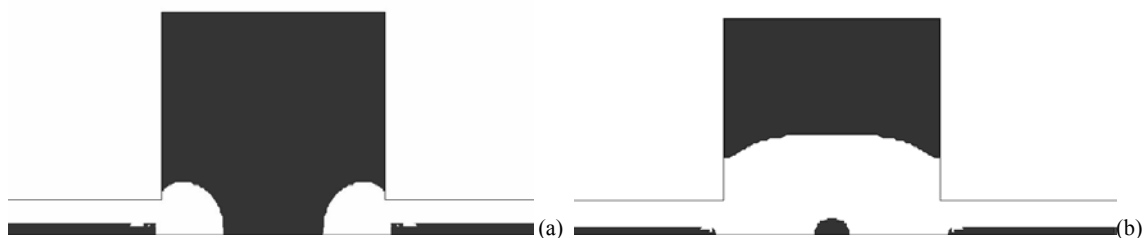
Figure 4. Sudden expansion and contraction flow with n=0.5: τ isobands for (a) J=1, and (b) J=10^2.

Initially, in Fig. 3(b), the mesh independence test may be found. The most sensible field was chosen to perform it, i.e., the pressure one. As may be noticed, only the coarser mesh presented a pressure drop quite different from the others meshes employed. Applying as a criterion to permit pressure drop differences of less than 3% between two consecutive meshes, the third mesh, namely MESH #3, has been chosen.
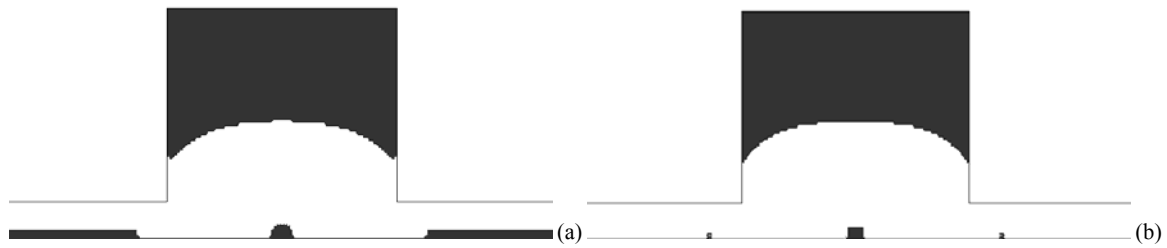
Figure 5. Sudden expansion and contraction flow with $n=0.5$: τ isobands for (a) $J=10^4$ and (b) $J=10^6$.

Next, in Fig. 4 and 5, τ isobands for $n=0.5$ and $J=1$, 10^2, 10^4 and 10^6, have been shown. In these figures, the black zones - characterized by $\tau < \tau_0$ - indicate the unyielded material regions, while the white ones – with $\tau > \tau_0$ - stand for the yielded material regions. As it may be observed, the unyielded regions decrease with the jump number growth; the larger the J value, the greater the regions subjected to very low shear rates tending to flow. Even more, while the J number increase has clearly affected the dead (stagnant) zones, its effect could be neglected in infinite viscosity regions. Certainly, the latter regions experienced such low shear rates that the J increasing was unable to force these material regions to flow. In the Fig.5(b), the J value was taken equal to 10^6 and the n maintained as 0.5. As shown in the figure, the very large jump value adopted was able to force all material regions to flow – even those subjected to extremely low shear rates, as the plug flows around the symmetry line and the region in the vicinity of the R_0 boundary.
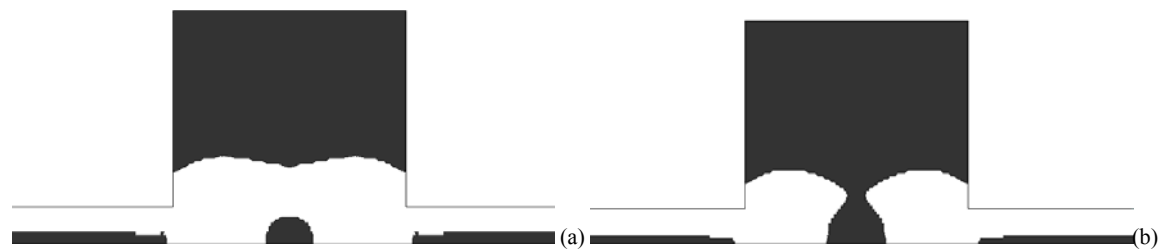
Figure 6. Sudden expansion and contraction flow for $J=12$: τ isobands for (a) $n=0.4$ and (b) $n=0.9$.

Finally, in Fig. 6, τ isobands for $n=0.4$ and 0.9, and $J=12$, have been shown. As expected, the unyielded material regions decrease with the diminishing of power-law index. This occurs because, when the power-law index decreases, the viscosity also decreases and consequently it will occur more regions subjected to high shear rate values.

4.3 A SMD fluid flow around a circular cylinder

In this section, in order to approximate the SMD fluid flows around a circular cylinder, a GLS formulation has been employed (Eq. (16)-(17)). The problem statement is shown in Fig. 7(a) for a system of Cartesian coordinate with origin at the channel outlet – as in the previous section, only one half of the domain has been simulated. They imposed boundary conditions for velocity it were a uniform parallel inlet velocity, free traction condition at channel exit, no-slip and impermeability on channel walls and cylinder surface, and symmetry condition at centerline ($\partial_2 u_1 = u_2 = 0$). In order to partition the computational domain Ω_h, 25,400 uniform bilinear finite elements (Q1/Q1) (25,901 nodal points) have been used – for the mesh detail around the cylinder, see Fig. 7(b)).
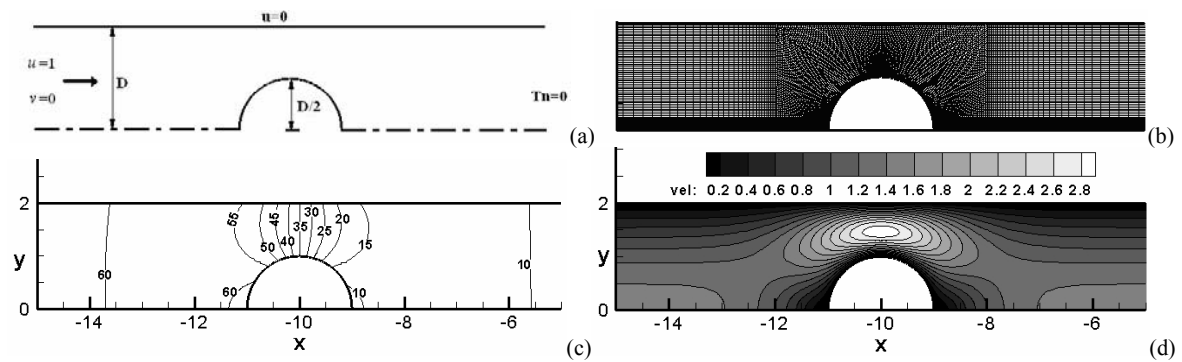
Figure 7. Newtonian fluid flow around a circular cylinder: (a) problem statement; (b) mesh detail; (c) pressure contours; (d) velocity isobands.

The problem aspect ratio was defined by the relationship between cylinder radius, $D/2$, and channel height, D, whch was taken as 1:2 in the numerical simulations. The jump number (Eq. (10)) was fixed as J=100 and the inlet dimensionless average velocity, $\bar{u}^* = \bar{u}/\dot{\gamma}_1\left(D/2\right)$ - with $\dot{\gamma}_1$ defined as in Eq. (9) - was ranged from 0.1 to 2.5. In order to calibrate the employed computational code, Figure 7 shows the pressure contours (Fig. 7(c)) and velocity isobands (Fig. 7(d)) for the inertialess flow of a Newtonian fluid around a circular cylinder. As it may be observed, the numerical approximations for velocity and pressure fields were in accordance with the classical literature (Slattery, 1999).
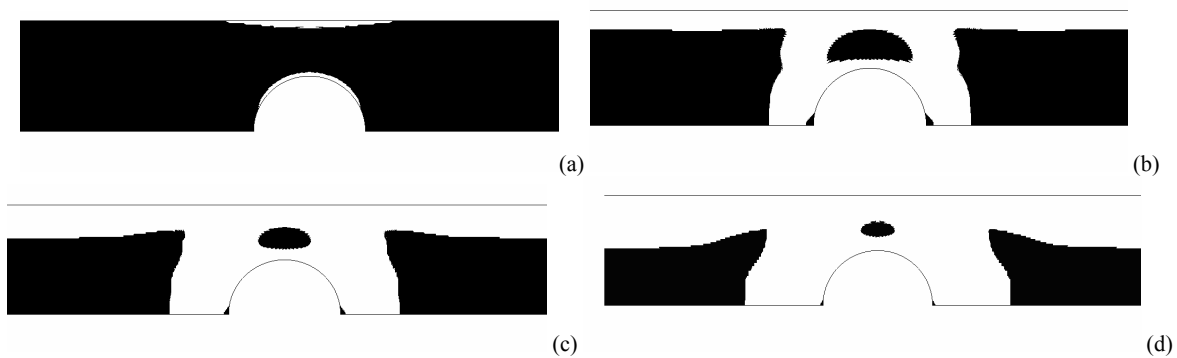
Figure 8. SMD fluid flow around a circular cylinder (J=100 and n=0.5): τ isobands for (a) $\bar{u}^*$ = 0.1; (b) $\bar{u}^*$=0.5, (c) $\bar{u}^*$=1.0; (d) $\bar{u}^*$=2.5.

In Figure 8 the influence of dimensionless average velocity $\bar{u}^*$ over the unyielded regions of the material (black zones in the figure) has been performed. In this figure, τ isobands were presented for J=100, n=0.5 and $0.1<\bar{u}^*<2.5$. First, the black regions represent high viscosity zones both downstream and upstream from the cylinder, and at the *vena contracta* formed between the cylinder surface and the channel wall. Second, τ isobands presented an axial symmetry with respect to the cylinder, which is in accordance with the theory of inertialess fluid flows. Further, the unyielded regions decrease with the growth of $\bar{u}^*$; while, for $\bar{u}^*$=0.1. (Fig. 8(a), the unyielded regions were strongly dominant, for $\bar{u}^*$=0.5, 1.0 and 2.5, the black zones plainly presented a decrease of $\bar{u}^*$ velocity values. This material behavior may be explained by the augmentation of the shear rate imposed by the growth of $\bar{u}^*$. By Equation (7), this growth implies that more regions will be subjected to shear stresses greater than the material limit stress, $\tau > \tau_0$.
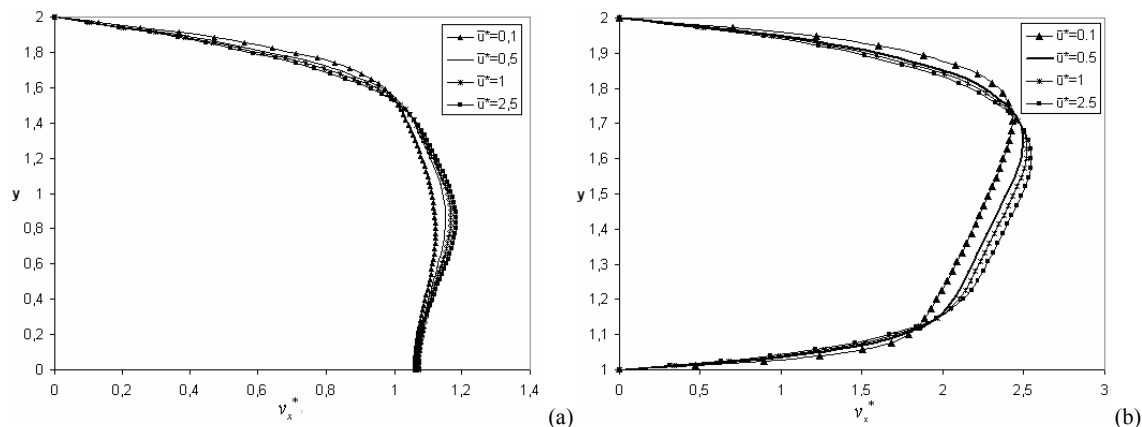
Figure 9. SMD fluid flow around a circular cylinder, for J=100 and n=0.5: v_x^* profile at (a) x=-12, (b) x=-10.

Figure 9 investigated the high viscosity regions mentioned above, showing the dimensionless axial velocity profiles, $v_x^* = v_x / \overline{u}^*$, for two different axial positions, namely x=-12 and -10. The first one was chosen upstream from the cylinder (Fig.9(a)) and the second at the *vena contracta* formed above the cylinder (Fig. 9(b)). Figure 9(a) illustrates two distinct material zones. The first one contains a boundary layer near the channel wall and the second an extremely high viscosity region near the centerline, which was weakly influenced by the presence of the cylinder downstream – for all velocities $\overline{u}^*$ investigated. The Figure 9(b) shows three different material regions; it may be observed two boundary layers - one near the channel wall and another near the cylinder surface - and a high viscosity region at the *vena contracta* above the cylinder, which was strongly affected by the cylinder surface – again, a behavior verified for all $\overline{u}^*$ velocities.

5. FINAL REMARKS

In this article, numerical simulations of stead-state inertialess viscoplastic fluids have been carried out. The mechanical model employed, defined by Eq. (11), was based on the mass and momentum conservative equations coupled to the SMD viscoplastic (Eq.(7)) model. In order to perform the numerical approximation of the mechanical model, a Galerkin least-squares method, defined by Eq. (16)-(17), has been used with equal-order bilinear Langrangean interpolations for velocity and pressure fields.

Numerical simulations of a SMD fluid flowing through a duct subjected to a sudden expansion followed by a sudden contraction and around a circular cylinder have been performed. For both flows, the GLS method was capable to generate stable approximations for the yielded and unyielded flow regions. For the first case, it was verified that the decreasing of the jump number has augmented the dead zones and plug flow regions and that the decrease of the power-law exponent has diminished those regions. For the second flow, it was observed that the increasing of the dimensionless average velocity of the fluid augment decrease the unyielded zones of the material.

6. REFERENCES

Astarita, G. and Marrucci. G., 1974, "Principles of Non-Newtonian Fluid Mechanics". v.1, John Wiley & Sons, U.S.A.

Bird, R. B., Armstrong, R. C. and Hassager, O., 1987, "Dynamics of Polymeric Liquids". v.1, John Wiley & Sons, U.S.A.

Ciarlet,P.G., 1978 "The Finite Element Method for Elliptic Problems". North Holland, Amsterdam.

Franca, L.P., and Frey, S., 1992. "Stabilized Finite Element Methods: II. The Incompressible Navier-Stokes Equations", Comput. Methods Appl. Mech. Eng., vol. 99, pp. 209-233.

Jurjevic, R., 1999. "Modelling of Two-Dimensional Laminar Flow Using Finite Element Method", International Journal for Numerical ethods in Fluids, vol. 31, pp. 601-626.

Souza Mendes, P.R. and Dutra E. S. S., 2004. "Viscosity Function for Yield-Stress Liquids", Applied Rheology, vol. 14, pp.296-302.

Souza Mendes, P.R. et al., 2007. "Flow of viscoplastic liquids through axisymmetric expansions- contractions", J. Non-Newtonian Fluid Mech, vol. 142, pp. 207–217.

Slattery, J.C., 1999. "Advanced Transport Phenomena", Cambridge University Press, Cambridge.